Experimental Characterization and Computer Vision-Based Detection of Pitting Corrosion on Stainless Steel

DUNCAN J. FURE, JESSICA LUU, REBECCA B. LI,
MICHAEL D. TODD and LONG WANG

ABSTRACT

Pitting corrosion is a form of corrosive damage that leaves cavities in metallic materials, which can significantly compromise structural safety and reliability. For instance, stainless steel, as a versatile structural material, can subject to pitting corrosion, regardless of its high corrosion resistance. The pit growth typically exhibits an initial high growth rate during nucleation, followed by an eventual saturation limit, which will ultimately lead to material failure. Although pitting corrosion is a prevalent damage mode, there is limited data on pit development under different corrosive conditions. Also, it remains challenging to efficiently detect pitting corrosion on large-scale water resources infrastructure. Therefore, this study aims to not only experimentally characterize the evolution of pit morphologies (i.e., depth and surface opening area), but also adopt computer vision techniques to detect pitting corrosion. In particular, an accelerated corrosion experiment was designed and implemented to introduce pitting corrosion to stainless steel in a controlled manner. The three-dimensional pit morphologies were measured using a high-precision laser scanner. Different statistical models were implemented to characterize the evolution of pit morphologies. Furthermore, this study also trained and compared several different computer vision algorithms to identify a promising structural health monitoring approach to detect pitting corrosion in a scalable and non-contact manner.

INTRODUCTION

Pitting corrosion, consisting of small cavities formed in metallic materials, is a dangerous form of corrosion that can be difficult to detect. After the protective layer on a material's surface fails, pitting develops due to the potential difference between an anode and a cathode (i.e., metal and ions, respectively), transferring current through a medium, usually water [1, 2]. The most common cause of this condition is the presence of chlorine ions, typically from a marine environment. Pitting is an autocatalytic

Duncan J. Fure, Jessica Luu, Rebecca B. Li, and Long Wang*, California Polytechnic State University, San Luis Obispo, CA, 93407, USA
Michael D. Todd, University of California-San Diego, La Jolla, CA, 92093, USA
*Corresponding author e-mail: lwang38@calpoly.edu

process, which means that once a pit forms, the conditions for the chemical reaction to continue are created within the pit and damage is localized [1-3]. Not all pits will continue growing at the same rate, and some will even stop growing.

The unique and dangerous effect of pitting corrosion is its potential for causing stress-corrosion cracking (SCC), which refers to cracks developed on corroded materials under mechanical loading. SCC can cause earlier structural failures, where localized damage results in the complete failure of a structural member. When pitting corrosion exists, a pit acts as the initiation point for a crack and intensifier of stress, leading the crack to propagate and ultimately cause material rupture [2]. Due to the small scales involved and effects of the microstructure of the material, it remains difficult to measure and determine where SCC may occur.

This study aims to conduct controlled and repeatable corrosion experiments to better understand how pits develop over time. In particular, 304 stainless steel was chosen as the subject material for accelerated pitting corrosion experiments, and the resulting pit shapes were measured with a high-resolution laser scanner. These pit shape measurements were then analyzed to determine their statistical distributions at different corrosion times and how they evolved over time. In addition, to achieve scalable detection and monitoring of pitting corrosion damage, different computer vision algorithms were developed and compared.

EXPERIMENTAL DETAILS

Accelerated Pitting Corrosion Experiment

The experimental method utilized in this study was built on the one previously developed by Muehler et al. [4]. To be specific, the experiment consisted of subjecting AISI 304 stainless steel specimens ($50.8 \times 342.9 \times 4.7625$ mm^3, purchased from Metals Depot) to a heated aqueous solution of iron (III) chloride ($FeCl_3$, purchased from Sigma-Aldrich) with a pH of 1. This was achieved by thoroughly dissolving 8.11 g of $FeCl_3$ for every 100 mL of deionized (DI) water until an appropriate amount of solution volume was reached. The solution was then heated to 50 °C and added to the inner chamber of a corrosion resistant container, as shown in Figure 1. The outside container was a heated water bath which helped maintain the temperature of the corrosive solution during the corrosion process. The steel specimens were first sanded appropriately and washed with DI water before being placed into the solution. The specimens were spaced at least 25.4 mm from each other with a three-dimensional (3D) printed fixture. Upon adding the corrosive solution, these specimens were corroded for different durations of time (i.e., 0.25, 0.5, 1, 2, and 3 hours) and then removed and washed with DI water.

To characterize the resulting pit morphologies, all corroded specimens were scanned with a Micro-Vu Vertex 312UC system that was equipped with a LSM4-2 laser distance scanner. A central region of 30×45 mm^2 on each specimen was measured with a resolution of ~4 μm in the X and Y directions.

Statistical Analysis of Pit Morphologies

The laser scan measurements were a 3D point cloud representative of the surface roughness of the samples. Based on the local slope steepness, points were organized as part of a pit. This collection of pits was then fitted to the function of a half ellipsoid shown in Equation (1).

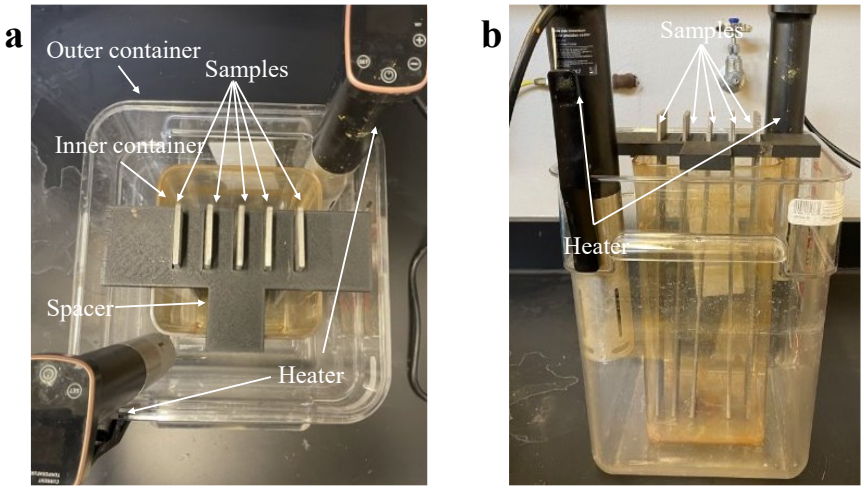

Figure 1. Test set-up of accelerated pitting corrosion for a) top view and b) side view.

$$\hat{z} = r_3\left(1 - R^2\left(\frac{\cos^2\hat{\theta}}{r_1^2} + \frac{\sin^2\hat{\theta}}{r_2^2}\right)\right) \quad (1)$$

The XY plane was established based on the average surface height, and the *(X, Y)* coordinates were represented by polar coordinates *(R, θ)*. All the variables with a caret indicate local coordinates, relative to the center of the ellipsoid. The values r_1, r_2, and r_3 are the length of the semi-axes in the X, Y, and Z directions, respectively. The advantage of this strategy over direct calculation based on raw measurements is that it could exclude any measurement error, such as occasionally erroneous points which appear much deeper than is physically possible. Based on the fitted ellipsoid functions, 3D pit morphologies (e.g., depth and surface opening area) could be effectively characterized. This paper focuses on investigating the distribution and growth of pit depth.

In addition, the understanding of the statistical distribution of pit depth can potentially enable predictions of pitting corrosion severity with a limited number of inspections. This requires the knowledge of the underlying probability distribution function (PDF), which may be determined by comparing experimental measurements with theoretical statistical model distributions. The more values observed, the more likely the true distribution can be identified. To determine the PDF, a histogram of all visible pits and their corresponding depths was generated for each corrosion time, and different statistical model distributions (e.g., normal, log-normal, beta, and Pearson Type III distributions) were fitted to the histogram using the least squares method. Furthermore, based on the data obtained from different corrosion times, an empirical model was generated to characterize how the distribution of pit depths evolved over time. The empirical model can potentially help establish a trend of pit growth, which was found to follow a power law, aligning with established research [5, 6].

COMPUTER VISION-BASED PITTING CORROSION DETECTION

We adopted computer vision techniques to achieve efficient binary classification of the existence of pitting corrosion. To be specific, four different ImageNet-pretrained convolutional neural networks (CNNs) were explored, which were GoogLeNet, MobileNet, ResNet-50, and EfficientNet. These models were selected based on a variety of factors, such as model size, efficiency, and their ability to capture small details needed

for our data. Each CNN was customized to accept 224 × 224 pixels image inputs, then had its output layer or final classifier replaced with a global average pooling layer, a fully connected layer, and a softmax activation, so it could learn from our stainless-steel image library. A total of 784 high-resolution images were labeled on whether they contained pits or not, forming the "*Pits*" and "*No Pits*" classes. There were 460 "*Pits*" images and 324 "*No Pits*" ones (i.e., pristine stainless-steel images). Data augmentation was applied, including horizontal and vertical flips, zooms, and rotations. 85% of the data was used for training, 10% for testing, and 5% for validation, stratified by class.

RESULTS AND DISCUSSION

Measurement and Statistical Analysis of Pit Morphologies

Pitting corrosion development and growth is a stochastic process subject to high variability. While many phenomenological models have been developed based on field or lab-controlled experiments, physics-based models for simulating pit growth are yet to be reliable [7-9]. This study proposes a model based on 10 samples generated at each corrosion time duration, totaling 50 samples.

Figure 2 shows two-dimensional (2D) contours of a sample after 3 hours of corrosion based on the laser scan data. Figure 2c illustrates an ellipsoid function fitted to the measurements of an individual pit shown in Figure 2b. For each corrosion time, since the corrosion conditions were the same for different samples, all pits generated were assumed to be independent and belong to the same dataset. Many different PDFs were utilized to characterize the statistical distribution of pit depths. Among them, three models, namely log-normal, beta, and Pearson Type III, were identified to provide relatively close fit to the experimental data. It is worth noting that literature also reported the application of normal and exponential distributions [7], of which was also evaluated in this study.

Figure 3 shows the normal distribution model fitted to the histograms of pit depth for different corrosion times. A normal distribution can be seen to be ill-fitting as it significantly underestimated the right tails of the distributions (i.e., deeper pits) for corrosion times of 1 hour and beyond. In addition, this study implemented quantile-quantile (Q-Q) plots to quantitively determine the model fitting quality. Essentially, a Q-Q plot visually compares empirical and theoretical quantiles with a perfect fit following a 45° titled line [10]. R^2 values could be used to quantify how close the Q-Q plots were to the 45° line. For the fitted normal distribution, Figure 4 shows its Q-Q plots for different corrosion times. One can observe a significant mismatch between the model prediction and experimental data from 1 hour or more of corrosion time, which

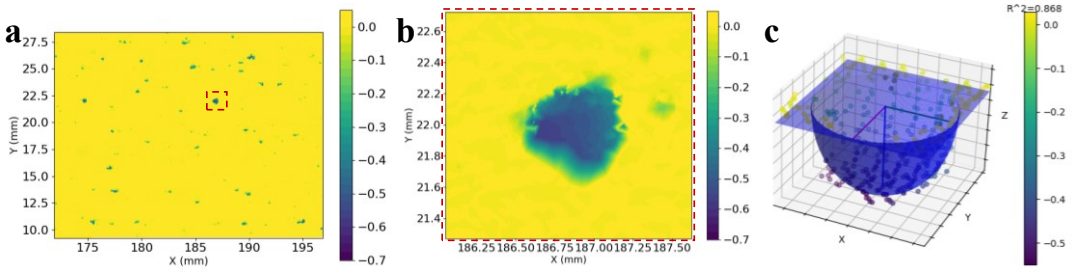

Figure 2. a) 2D color contour plot of pit morphology of a sample after 3 hours of corrosion. b) A zoomed-in view of a single pit. c) a 3D view of the pit shown in b) with a fitted ellipsoid function.

further confirmed that the normal distribution could not accurately represent pit depth distributions.

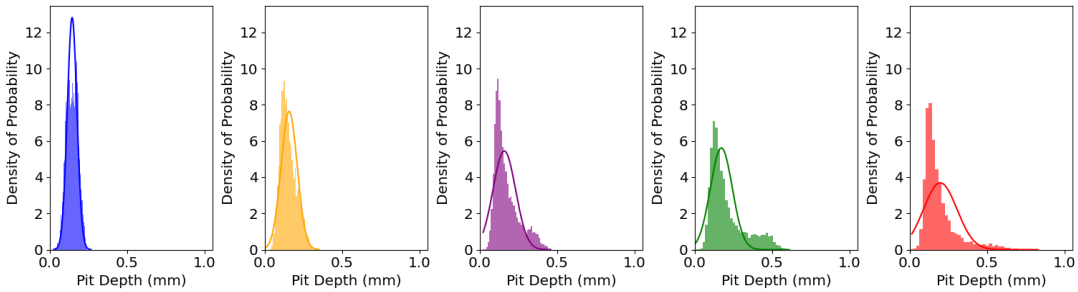

Figure 3. Comparison of histograms of pit depth to normal distribution for 0.25-, 0.5-, 1-, 2-, and 3-hour samples (in left-to-right order).

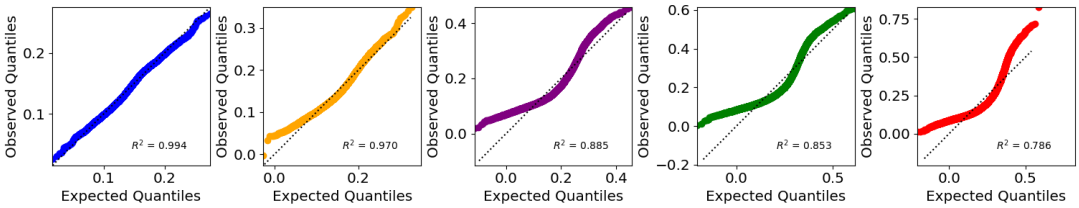

Figure 4. Q-Q plots of fitted normal distribution for 0.25-, 0.5-, 1-, 2-, and 3-hour samples (in left-to-right order).

On the other hand, Figure 5 shows the Pearson Type III model fitted to all experimental data, which exhibited a much better fitting than the normal distribution. The quality of the fit of this distribution was evaluated with the corresponding Q-Q plots shown in Figure 6. The overall fitting was good, except for experimental data from 1 and 2 hours of corrosion. In fact, it is interesting to note that both the 1-hour and 2-hour corrosion times' histograms showed a secondary peak that could not be captured with single modal distributions like the Pearson Type III function. Furthermore, the R^2 values for each corrosion time of the considered distributions are summarized in Table I. Three distributions, including log-normal, beta, and Pearson Type III, all could describe the underlying distribution of the data with similarly high accuracy.

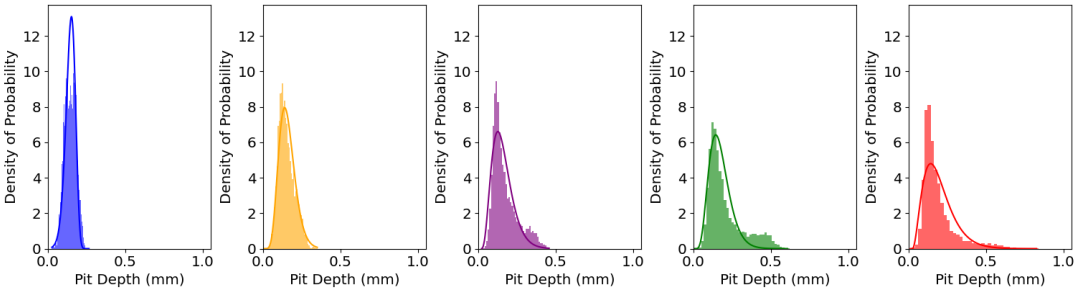

Figure 5. Comparison of histograms of pit depth to Pearson Type III distribution for 0.25-, 0.5-, 1-, 2-, and 3-hour samples (in left-to-right order).

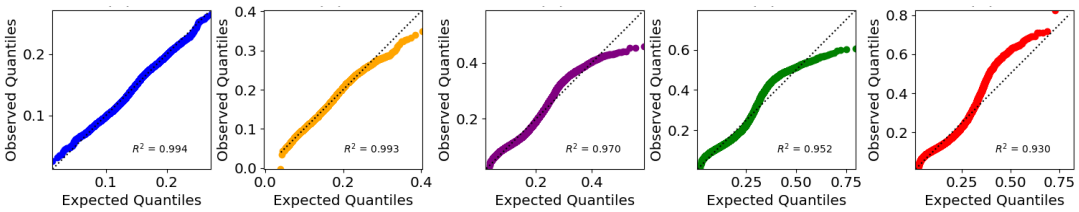

Figure 6. Q-Q plots of fitted Pearson Type III distribution for 0.25-, 0.5-, 1-, 2-, and 3-hour samples (in left-to-right order).

However, the 2 and 3-hour corrosion time datasets could not be fit accurately by any distribution, especially for the right tail of the distribution. This could be attributed to the highly stochastic nature of the pitting corrosion process or it might suggest that a different distribution or combination of distributions is required for more accurate modeling. To enhance the significance of the results, additional data collection could be considered.

Pit Morphology Development

Theoretically, the deepest pits are most dangerous for structural integrity, as they are more likely to be the initiation of SCC damage. To simplify analysis and focus on the deepest pits, only the 99th percentile of pits' depths will be considered. Note that the percentile of the data can be found nonparametrically and does not rely on the underlying distribution. This is useful as the right tail of the distribution is most relevant for predicting the deepest pits. Here, the 99th percentile was determined using the NumPy *percentile* function, where the cumulative distribution function was interpolated linearly. The progression of the 99th percentile data could be established as a function of time to develop an empirical relationship as depicted in Figure 7. This can be useful in understanding how the deepest pits (i.e., the initiation points of failure) will likely develop with time.

TABLE I. R^2 VALUES OF THE Q-Q PLOTS FOR DIFFERENT STATISTICAL MODELS

Statistical Models	**0.25 hr**	**0.5 hr**	**1.0 hr**	**2.0 hr**	**3.0 hr**	**Average**
Exponential	0.800	0.910	0.957	0.948	0.980	0.919
Normal	0.994	0.970	0.884	0.852	0.786	0.897
Log-Normal	0.994	0.992	0.969	0.936	0.949	0.968
Beta	0.997	0.994	0.959	0.931	0.912	0.958
Pearson Type III	0.994	0.993	0.970	0.952	0.930	0.968

To be specific, for the 10 samples at each corrosion time, a 99th percentile was calculated for the pit depth. The average of these 99th percentiles data ($P_{99,avg}$) was shown as a point in Figure 7, with the error bars representing their standard deviation. Empirically, the data followed the power law equation described in Equation (2),

$$P_{99,avg} = at^b \tag{2}$$

where a and b are model fitting parameters, and t is the corrosion time duration. The value of b was between 0 and 1, which means that pit depths grew non-linearly with time, with each successive hour resulting in a less increase in pit depth. More data needs to be collected to determine if this trend continues with time or if the corrosion reaches a saturation point where corrosion no longer results in deeper pits.

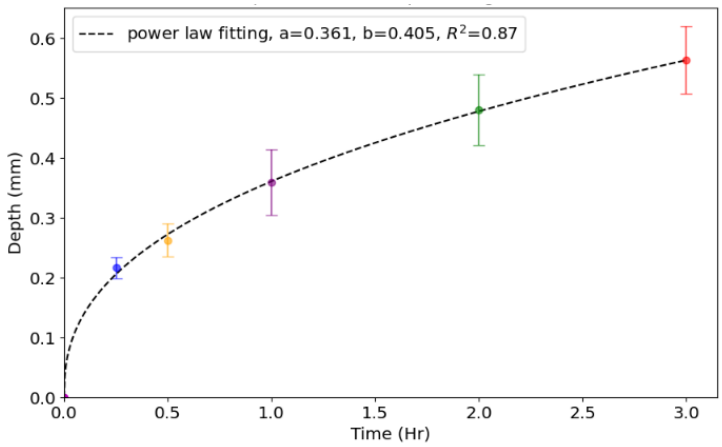

Figure 7. Evolution of the 99th percentile pit depths of 0.25-, 0.5-, 1-, 2-, and 3-hour samples.

Computer Vision-Based Pitting Corrosion Identification

The training and validation accuracies obtained by the four CNNs for binary pit detection are summarized in Table II. GoogLeNet achieved the highest performance with 90.04% training accuracy and 85.10% validation accuracy, followed by MobileNet at 85.02%/80.0%. The results indicate that GoogLeNet's Inception modules were most effective at capturing the pits at different scales compared to the other models.

TABLE II. TRAINING AND VALIDATION RESULTS FOR BINARY PIT DETECTION

CNN Models	Final Training Accuracy	Final Validation Accuracy
GoogLeNet	90.04%	85.10%
MobileNetv2	85.02%	80.00
ResNet-50	84.97%	75.00%
EfficientNet-B0	82.43%	75.85%

CONCLUSION

This study experimentally investigated pitting corrosion damage on 304 stainless steels. The evolution of pit morphologies was quantitatively characterized, indicating that pit depths grow non-linearly over time, specifically following a power law equation with high significance. Among the statistical models describing the distribution of the pit depth population, log-normal, beta, and Pearson Type III distributions demonstrated strong fitting accuracy, though the high stochastic nature of corrosion might cause uncertainty in the experimental data. Furthermore, this study also adopted and compared several CNN models to detect the existence of pitting corrosion in an efficient and scalable manner. GoogLeNet was found to possess the highest performance.

ACKNOWLEDGEMENT

This research is supported by the United States Army Corps of Engineers and Engineer Research and Development Center Cooperative Agreement W9132T-22-2-0014.

REFERENCES

1. Verma, C., Aslam, J., Aslam, R., Zehra, S., Chaudhery, & M. H.. (2023) *Handbook of Corrosion Engineering: Modern Theory, Fundamentals and Practical Applications*. Elsevier.
2. McCafferty, E. (2010). *Introduction to Corrosion Science*. Springer New York.
3. Abood, T. H.. (2008). *The influence of various parameters on pitting corrosion of 316L and 202 stainless steel*. Master's Thesis, Engineering of the University of Technology.
4. Muehler, R. J., Venz, J. B., Todd, M. D., & Wang, L. (2023). Experimental characterization and computer vision-assisted detection of pitting corrosion on stainless steel structural members. *Proceedings of the 14th International Workshop on Structural Health Monitoring*.
5. Katano, Y., Miyata, K., Shimizu, H., & Isogai, T. (2003). Predictive model for pit growth on underground pipes. *Corrosion*, *59*(2), 155–161.
6. Paul, S. (2016). Modeling unpredictable failures of 304 construction material in seawater by pitting corrosion and simulate chloride ion distribution by finite element method. *Multidiscipline Modeling in Materials and Structures*, *12*(3), 543–557.
7. Melchers, R. E. (2005). Statistical characterization of pitting corrosion—part 2: Probabilistic modeling for maximum pit depth. *Corrosion*, *61*(8), 766–777.
8. Caleyo, F., Velázquez, J. C., Valor, A., & Hallen, J. M. (2009). Markov chain modelling of pitting corrosion in underground pipelines. *Corrosion Science*, *51*(9), 2197–2207.
9. Garbatov, Y., Zayed, A., Wang, G., Melchers, R., & Paik, J. (2005). Non-Linear Corrosion Model for Immersed Steel Plates Accounting for Environmental Factors. Discussion. *Soc. Nav. Archit. Mar. Eng., Trans.*, *113*, 306-329.
10. Klemela, J. (2009). *Smoothing of multivariate data : density estimation and visualization* (1st ed.). John Wiley & Sons.